Scalings of Ion-Temperature-Gradient-Driven Anomalous Transport in Tokamaks

A. M. Dimits, T. J. Williams, J. A. Byers, and B. I. Cohen
Lawrence Livermore National Laboratory, P.O. Box 808, Livermore, California 94550
(Received 30 October 1995)

Results are presented from the first systematic nonlinear gyrokinetic simulation study of the scalings and parameter dependences of toroidal ion-temperature-gradient-driven (ITG) turbulence and transport in large magnetic-fusion-relevant tokamaks. Such simulations are made possible by significant advances in computational physics algorithms which are summarized. The simulated ion-thermal transport rates have clear "gyroreduced Bohm" scaling and are too low to account for the anomalous transport seen in the outer half of some TFTR *L*-mode discharges, indicating that additional mechanisms, such as nonadiabatic-electron effects, are operative. [S0031-9007(96)00511-X]

PACS numbers: 52.35.Ra, 52.25.Fi, 52.55.Fa, 52.65.Tt

We report results from the first systematic nonlinear gyrokinetic simulation scaling and parameter studies of tokamak turbulence and transport in large present-day tokamaks. This work treats turbulence driven by the toroidal ion-temperature-gradient-driven (ITG) instability [1].

Transport of heat, particles, and momentum in tokamaks is often observed to be much larger than predicted by laminar collisional theories [2]. While the cause of this "anomalous" transport is generally believed to be turbulence driven by instabilities, quantitative theories with both predictive capability and a sound footing in first-principles physics are still under development, although a recent ITG-turbulence transport model [3] based on linear gyrokinetic and nonlinear "gyrofluid" [4] simulations shows promise.

Analytical theories of tokamak transport [1,5–7] either rely on unproven assumptions that strongly affect the conclusions or else have a very small parameter-space region of true validity and are therefore applied outside this region of validity. They must therefore be tested by either numerical simulations or by adequately diagnosed experiments.

The most sophisticated noncollisional fluid simulations use 6-fluid-moment gyrofluid models [3,8], whose nonlinear validity is not known *a priori*. Since the toroidal ITG mode is a kinetic instability [1], some demonstration of the validity of the fluid representations of the *nonlinearities* in the gyrofluid models is important. Results from 4-moment [8,9] and 6-moment [8] gyrofluid simulations disagree sufficiently that they fail to show that convergence in the gyrofluid hierarchy has been achieved with 6 moments. Thus, nonlinear (gyro)kinetic simulations remain an important test for gyrofluid models.

The gyrokinetic equations are valid nonlinearly, but are more challenging to simulate. It has taken the combination of several advances in computational algorithms, namely, nonlinear gyrokinetic simulation methods [10], δf algorithms [11,12], the "quasiballooning-coordinate" numerical representation [13], and flux-tube simulation domains [8,14] to make particle-based kinetic simulation a practical tool for direct studies of turbulence and anomalous transport in tokamaks. This combination is a new aspect of our work.

The physical model used is electrostatic, with a single fully toroidal nonlinear gyrokinetic ion species [15] that has equilibrium temperature, density, and velocity gradients:

$$\frac{\partial \delta g}{\partial t} + v_\parallel \nabla_\parallel \delta g + \mathbf{V}_{\rm dr} \cdot \boldsymbol{\nabla}_\perp \delta g = [(\mathbf{v}_* - \mathbf{v}_d) \cdot \boldsymbol{\nabla}_\perp - v_\parallel \nabla_\parallel] \frac{Ze}{T_i} \overline{\phi} F_M , \tag{1a}$$

$$\mathbf{V}_{\rm dr} = \mathbf{v}_d + \mathbf{v}_{EB} + V_0'(r - r_0)\hat{\boldsymbol{\theta}} , \tag{1b}$$

$$\frac{dv_\parallel}{dt} = -(v_\perp^2/2\Omega_i)\boldsymbol{\nabla}\Omega_i , \tag{1c}$$

$$\mathbf{v}_* = -\frac{cT_i}{ZeB}\hat{\mathbf{b}} \times \hat{\mathbf{r}} \frac{1}{L_T}\left[\frac{1}{\eta_i} + \left(\frac{v^2}{2v_{\rm ti}^2} - \frac{3}{2}\right)\right] + \frac{1}{L_v}\frac{v_\parallel}{v_{\rm ti}^2} . \tag{1d}$$

Here, δg is the perturbed ion gyrocenter distribution function, $-e$ is the electron charge, Ze and m_i are the ion charge and mass, B is the magnetic field strength, $\hat{\mathbf{b}}$ is the unit vector in the magnetic field direction, $\Omega_i \equiv ZeB/m_i c$ is the ion gyrofrequency, $\boldsymbol{\nabla}_\parallel \equiv \hat{\mathbf{b}} \cdot \boldsymbol{\nabla}$, $v_\parallel \equiv \hat{\mathbf{b}} \cdot \mathbf{v}$, $v = |\mathbf{v}|$, $\mathbf{v}$ is the particle velocity, V_0' is an externally imposed $\mathbf{E} \times \mathbf{B}$ velocity shear, r is the (gyrocenter) minor radius, L_T is the temperature gradient scale length, $\eta_i \equiv L_n/L_T$, L_n is the density gradient scale length, $v_{\rm ti}/L_v$ is an externally imposed parallel velocity shear, $v_{\rm ti} \equiv \sqrt{T_i/m_i}$, and T_i is the ion temperature. Also, $\mathbf{v}_d$ is the sum of the magnetic curvature and $\boldsymbol{\nabla}B$ drifts, and $\mathbf{v}_{EB}$ is the gyroaveraged $\mathbf{E} \times \mathbf{B}$ drift of the gyrocenters. A low-β circular-cross-section model equilibrium is used.

Equation (1a) is solved using the partially linearized δf particle method [11,12], with four-point gyroaveraging [10]. The electrostatic potential ϕ is obtained from a gyrokinetic Poisson equation [10]. The electron response

is taken to be adiabatic, with a zero response to the flux-surface-averaged potential [16].

The main free energy source for instability is the ion temperature gradient. Self-generated turbulent-Reynolds'-stress-driven flows, along with their dominant collisionless damping [17] are included fully and self-consistently in the gyrokinetic model. External sheared parallel, $\mathbf{E} \times \mathbf{B}$, or toroidal flows are also included, if needed.

The simulation domain used is a flux tube of small perpendicular extent, but which spans one or more poloidal circuits in the parallel direction. If r is the minor radius, ζ is the toroidal angle, and θ is a poloidal straight-field-line coordinate angle, this domain can be expressed as $\rho_i \ll \Delta r \ll L_T$, $-\pi M_\theta \le \theta \le \pi M_\theta$, $\Delta\zeta = 2\pi/M_\zeta$, where $\rho_i \equiv v_{\mathrm{ti}}/\Omega_i$ is the thermal ion gyroradius, and M_θ and M_ζ are integers. The flux tube is taken to the periodic in ζ, i.e., the periodicity interval is $2\pi/M_\zeta$.

The field quantities in the code are defined on a quasiballooning-coordinate grid [13]. Suitable quasiballooning coordinates are (r, y, z), where

$$y \equiv -\frac{r_0}{q_0}[\zeta - \hat{q}\theta - V_0'(r - r_0)tq_0/r_0], \quad (2a)$$

$$z \equiv q_0 R_0 \theta\,. \quad (2b)$$

Here r_0 is the minor radius at the center of the simulation domain, $q_0 = q(r_0)$ where $q(r)$ is the magnetic safety factor, and R_0 is the major radius at the minor axis. $\hat{q}$ is defined by dividing the y domain into N_ζ equally spaced intervals in the flux tube ($M_\zeta N_\zeta$ in the whole tokamak), and setting $\hat{q}(r) = m(r)/(M_\zeta N_\zeta)$where, at each radial surface r, $m(r)$ is the integer that makes $\hat{q}$ closest to $q(r)$. For any $q(r)$ profile, this choice allows the constant-β grid lines to connect exactly to (generally different) grid lines across the parallel boundaries of the simulation domain while maintaining the true physical periodicity [13]. The velocity-shear term in Eq. (2a) minimizes the motion of particles past grid cells.

The parallel derivative in quasiballooning coordinates is

$$\nabla_\parallel = \frac{\partial}{\partial z} + \epsilon_B(q - \hat{q})\frac{\partial}{\partial y}\,, \quad (3)$$

where $\epsilon_B = r_0/R_0$. Our choice of $\hat{q}$ guarantees that the second term is typically much smaller than $\nabla_\parallel$, so that parallel wave number spectrum is uniformly and optimally packed for all values of r. The component of the perpendicular derivative within a flux surface is $\nabla_y = \partial/\partial y$. The elongation of the fluctuations along the magnetic field renders terms resulting from the nonorthogonality of y and z negligible. The radial differences, interpolation, deposition, and smoothing are formed using shapes in *configuration* space (not ballooning-coordinate space) that are independent of poloidal location [13]. This choice prevents grid collapse and resolution loss in the presence of magnetic and velocity shear, and is necessary to allow a smooth implementation of the toroidal periodicity condition across the parallel boundary.

Profile relaxation [16] is prevented by making the simulation volume periodic in r at fixed y, generalizing Kotschenreuther's twist-shift radial periodicity condition [12] to give a seamless radial connection even in the presence of external velocity shear.

Using a Pade approximation for the Bessel functions [4], we have derived an accurate (to within 5% for $k_\perp \rho_i < 3$, where $k_\perp$ is the perpendicular wave number) and easily solved approximation (given for the case of equal electron and ion temperatures in Ref. [18]) to the gyrokinetic Poisson equation of Ref. [16]. A direct Fourier-in-y, tridiagonal-in-r elliptic solver that takes into account the twisting of the quasiballooning coordinates is used to solve the resulting second-order elliptic PDE. Further grid-based smoothing is applied to ϕ.

A systematic study of the scalings and parameter dependence of toroidal ITG turbulence and transport has been completed using our code. The parameter values were varied one at a time from a base simulation case which represents conditions in a TFTR L-mode discharge (TFTR shot #41309) at $r = 0.5a$, where a is the minor radius of the last closed flux surface. These parameter values are $\eta_i = 4$, $q_0 = 2.4$, $\hat{s} \equiv (r_0/q_0)dq/dr = 1.6$, $\epsilon_T \equiv L_T/R_0 = 0.1$, $\epsilon_B = 0.2057$, and $\tau = T_e/T_i = 1$. Typical numerical parameters are time step $dt = 0.2L_T/c_s$, where $c_s \equiv \sqrt{T_e/m_i}$, particle number $N_p = 4 \times 10^6$, perpendicular grid sizes $\Delta_x = \Delta_y = 0.8\rho_s$, and grid cell numbers $N_x = N_y = 128$, and $N_z = 32$. The spatial smoothing represents an effective Fourier-space form factor $\exp[-(a_y k_y \Delta_y)^4]/\{[1 + (a_x k_x \Delta_x)^4][1 + (a_z k_z \Delta_z)^4]\}$, typically with $a_x = a_y = 1.25$, and $a_z = 1$. The radial (x) smoothing is in the physically radial (∇r) direction, and not along a line of constant y and z.

The linear phase of the simulation shows radially elongated structures with a perpendicular wave number characteristic of the fastest growing mode The structures seen in the nonlinear phase have comparable radial and poloidal correlation lengths at scales ($k_y \rho_s \sim 0.1$ for the base case) characteristically longer than the wavelength of the most unstable mode. The thermal flux typically has small relative ($\sim$10%) fluctuations on time scales of the order of the growth rate of the most unstable mode about a clear mean. We average over many such fluctuations in the results discussed below.

Convergence has been checked extensively and appears to be adequate with respect to particle number, grid and particle sizes in all three directions, the timestep, and the number of poloidal circuits traversed by the flux tube. (Additional checks simultaneously changing more than one numerical parameter at a time are still highly desirable, and will become possible with a massively parallel version of our code that is presently under development.) A summary of results showing convergence with respect to

the parallel resolution, the number of poloidal circuits traversed by the flux tube, and the box size is shown in Fig. 1. The thermal diffusivity is defined as

$$\chi_i = \frac{2L_T}{3} \sum_j \frac{v_j^2}{c_s^2} \mathbf{V}_{\rm dr} \cdot \hat{\mathbf{x}}, \tag{4}$$

where v_j is the velocity of particle j and the sum is over all of the simulation particles. (Note that a conductivity, equal to $1.5\chi_i$, is also commonly used, e.g., Ref. [19].) For sufficiently large box sizes, which are still significantly shorter than typical profile scale lengths, $\chi_i/\chi_{\rm GB}$, where $\chi_{\rm GB} \equiv \rho_s^2 c_s/L_T$, is finite and becomes independent of the box size. The transport therefore has a clear gyroBohm scaling, irrespective of the magnetic shear.

Self-generated perpendicular flux-surface-averaged $\mathbf{E} \times \mathbf{B}$ flows form in the nonlinear phase, and evolve on similar time scales and radial spatial scales to those of the turbulence. Their time scales are much more rapid than the ion bounce time and typical ion collision frequencies. The associated flow shear regulates the turbulence levels and transport rates. For the base-case parameter set, zeroing out the self-generated flows gives a saturated state with $\chi_i \simeq 6\chi_{\rm GB}$, or roughly 7 times larger than with the self-generated flows. Thus, the transport rate can be affected strongly not only by the instability physics, but also by additional flow damping mechanisms.

For a small number of simulation runs in which we have diagnosed them, including the base case, the relative fluctuations levels of the fluid field quantities are observed typically to have the ratios $\tilde{T}_{i\perp}/T_i \sim 3 - 4\tilde{T}_{i\parallel}/T_i \sim 1.5\tilde{n}/n_0 \sim 1.5 - 2\tilde{v}_{i\parallel}/c_s$. The smallness of $\tilde{v}_{i\parallel}$ is consistent with the toroidal ITG drive mechanism which is not mediated by parallel flow.

From the results of many simulation runs in which the physical parameters were varied individually about the base case parameter set, the thermal diffusivity is most simply normalized as

$$\chi_i \simeq 9 \frac{\rho_s^2 c_s}{R_0} \hat{\chi}(q/\epsilon_T, \eta_i, L_s/L_T, \tau, \epsilon_T, \epsilon_B, V'_\zeta L_T/c_s), \tag{5}$$

where $L_s = qR_0/\hat{s}$ is the magnetic shear length, and V'_ζ is the *toroidal* velocity shear.

The dependence of $\hat{\chi}$ on each of q/ϵ_T, η_i, L_x/L_T, and ϵ_T, with the other parameters set at the base-case values, are shown in Fig. 2. The τ and ϵ_B dependences of $\hat{\chi}$ (not shown) are weak. Large excursions in the physical parameters from the baseline are needed to produce even moderate increases in $\hat{\chi}$ above 1. Thus, for minor radii $r/a > 0.5$, the overriding dependence of the simulated χ_i on the minor radius is a strong decrease through the $\rho_s^2 c_s/R_0$ factor in Eq. (5).

For the base case, the simulation value ($\hat{\chi} = 1$) is a factor of almost 1.5 lower than the experimental value. At $r/a = 0.8$, the disagreement between our simulation and the experiment is greater than a factor of 8. The disagreements in χ_i have been translated into disagreements in T_i through a simple power-balance analysis. The power flow allowed by an upper bound to our simulated χ_i is balanced with the experimentally measured power flow. This gives a lower bounds for the predicted T_i which lies clearly above the experimental T_i for $r/a > 0.6$. A similar situation holds for some other TFTR discharges, including some *H*-mode shots. Thus *additional* physics beyond what is contained in the gyrokinetic ITG model, for example, electron kinetic destabilization or additional flow damping, is necessary to account for these experimental results. It is important to identify this additional physics. We have

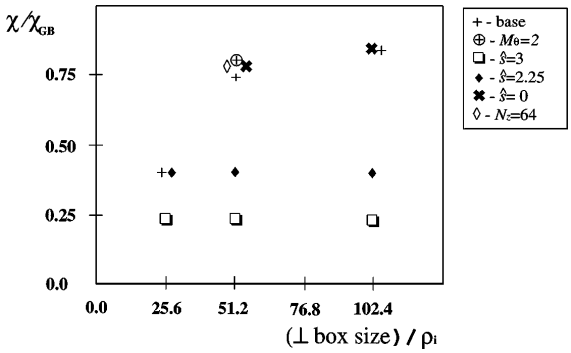

FIG. 1. Dependence of the normalized thermal diffusivity on the perpendicular box size, for various values of η_i, and $\hat{s}$. The physical parameters are as for the base case with the possible exception of one parameter, as given in the legend. Additional convergence results are also shown; $M_\theta = 2$ refers to a run using a flux tube that spans two poloidal circuits. This and the $N_z = 64$ (for which $a_z = 1$) run had the same physical parameters and simulation particle per grid cell density as the base case.

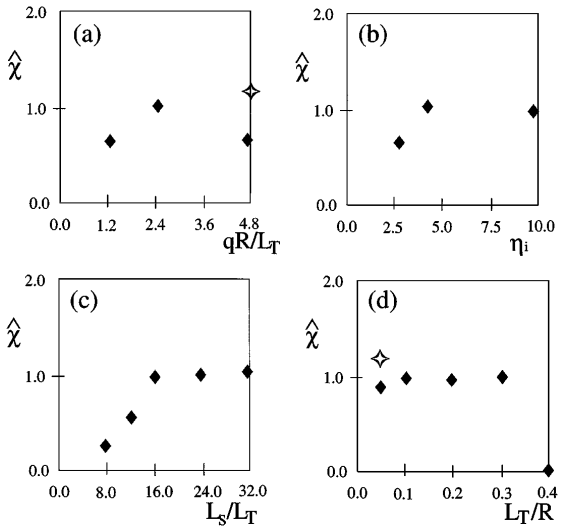

FIG. 2. Closed points show the dependence of $\hat{\chi}$ as defined in Eq. (5) diffusivity on (a) q/ϵ_T, (b) η_i, (c) L_s/L_T, and (d) L_T/R. On each plot, only the selected parameter in Eq. (5) is varied, and the other parameters are held at the base-case values. Open points show in (a) the results for $q = 4.8$, $\epsilon_T = 0.1$, $\hat{s} = 1.5$ and in (d) the results for $q = 2.4$, $\epsilon_T = 0.05$, $\hat{s} = 1.5$.

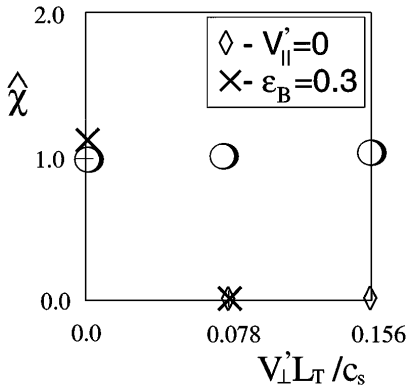

FIG. 3. Dependence of ion thermal conductivity on the rotation shear. Open diamonds are for purely $\mathbf{E} \times \mathbf{B}$ shear; other cases are for toroidal rotation shear (i.e., $V'_{\|}\epsilon_B/q + V'_{\perp} = 0$, where $V'_{\|} = v_{\rm ti}/L_v$, and $V'_{\perp} = V'_0$).

examined some L-mode discharges for which the lower bound predicted T_i is consistent with the experiment. In such cases, a more detailed examination based purely on ITG turbulence may be fruitful.

Results from the gyrofluid simulations of Ref. [3], which agree with experiments, do not agree with our gyrokinetic results. The disagreements in predicted temperature profiles become greater with increasing minor radius, corresponding to increasing departure from marginal stability. The main difference in the turbulent χ_i has been isolated as an overall factor of 2. Additionally, different scalings with q at fixed $\hat{s}$ and with ϵ_T at fixed η_i and q are observed. However, other gyrofluid simulation results [9] appear to be consistent with our results. Thus, discrepancies remain that are not fully understood. To resolve the origin of these discrepancies we are (a) collaborating with the authors of Ref. [3] to remove the differences in our numerical representations and to further check numerical convergence, and (b) developing a semiempirical theoretical criterion for the validity of the gyrofluid equations as an approximation to the gyrokinetic equations for toroidal ITG turbulence.

Toroidal flow shear is an important ingredient in many tokamaks, due to the presence of an external torque from neutral beams, and has different effects in different tokamaks [19]. The present code can address toroidal-rotation effects in TFTR. The dependence of $\hat{\chi}$ on V'_{ζ}, with other parameters as for the base case, is shown by the circles in Fig. 3. They show that toroidal flow shear can have a weak net effect on the ion thermal transport, in agreement with TFTR results, even when its $\mathbf{E} \times \mathbf{B}$ component alone (diamonds in Fig. 3) is highly stabilizing. This result, however, is strongly dependent on the pitch $B_\theta/B_\zeta = q/\epsilon_B$ of the magnetic field lines. When B_θ/B_ζ is increased (crosses), the toroidal flow shear can become stabilizing. The toroidal momentum diffusivity [χ_v, defined analogously by Eq. (4)] is found to be from 0.4 to 0.7 times χ_i. In the experiments [19], $\chi_v/\chi_i \simeq 1$–1.5, with χ_i normalized as in Eq. (4). We consider this a moderate disparity.

In summary, we have completed a systematic gyrokinetic simulation study ITG turbulence with global parameters in the regime of fusion-relevant tokamaks. GyroBohm scaling is observed, and the transport rates are too low to account for some TFTR L-mode discharges.

It is a pleasure to acknowledge beneficial discussions with A. H. Glasser, S. C. Cowley, S. E. Parker, G. W. Hammett, P. N. Guzdar, J. F. Drake, J. U. Brackbill, W. Dorland, R. H. Cohen, J. L. Milovich, and X. Q. Xu. We also thank G. W. Hammett for a careful and critical reading of the manuscript. The ITG simulations were performed on the NERSC C-90 computer under the SPP program. This work was performed under the auspices of U.S. Department of Energy (DOE) by Lawrence Livermore National Laboratory under Contract No. W-7405-ENG-48, and is part of the Numerical Tokamak Project supported by the High Performance Computing and Communications Program in the U. S. DOE.

[1] W. Horton *et al.,* Phys. Fluids **24**, 1077 (1981); J. Y. Kim *et al.,* Phys. Fluids **4**, 152 (1992).
[2] See, for example, T. C. Luce *et al., Proceedings of the 15th International Conference and Controlled Nuclear Fusion 1994* (IAEA, Vienna, 1995).
[3] W. Dorland *et al., Proceedings of the 15th International Conference on Plasma Physics and Controlled Nuclear Fusion, 1994.*
[4] G. W. Hammett *et al.,* Phys. Fluids B **4**, 2052 (1992).
[5] M. H. Redi *et al.,* Nucl. Fusion **27**, 2001 (1987).
[6] R. Z. Sagdeev and A. A. Galeev, in *Nonlinear Plasma Theory,* revised and edited by T. M. O'Neil and D. L. Book (Benjamin, New York, 1969).
[7] P. W. Terry *et al.,* Phys. Fluids **31**, 2920 (1988).
[8] M. A. Beer, Ph.D. Thesis, Princeton University, 1995.
[9] R. E. Waltz *et al.,* Phys. Plasmas **1**, 2229 (1994).
[10] W. W. Lee, J. Comput. Phys. **72**, 243 (1987).
[11] A. M. Dimits, Ph.D. thesis, Princeton University, 1988 (unpublished).
[12] M. Kotschenreuther *et al.,* in *Proceedings of the 14th International Conference on Plasma Physics and Controlled Nuclear Fusion, 1992* (IAEA, Vienna, 1993), Vol. 2, p. 11.
[13] A. M. Dimits, Phys. Rev. E **48**, 4070 (1993).
[14] P. N. Guzdar *et al.,* Phys. Fluids B **5**, 3712 (1993).
[15] E. A. Frieman and Liu Chen, Phys. Fluids **25**, 502 (1982).
[16] B. I. Cohen *et al.,* Phys. Fluids B **5**, 2967 (1993).
[17] T. H. Stix, Phys. Fluids **16**, 1260 (1973).
[18] A. M. Dimits and B. I. Cohen, in *Proc. IAEA Technical Committee Meeting on Advances in Simulation and Modeling of Thermonuclear Plasmas (1933, IAEA, Vienna).*
[19] S. D. Scott *et al.,* Phys. Rev. Lett. **64**, 531 (1990); T. H. Osborne *et al.,* Nucl. Fusion **35**, 23 (1995).